Characterizing incipient motion of low fines content soils with varying compositions, water contents, and relative densities

Mahsa Ghazian Arabi, Ali Farhadzadeh*

Department of Civil Engineering, College of Engineering and Applied Sciences, Stony Brook University, Stony Brook, NY 11794-4424, USA

***Corresponding Author.**
Email: ali.farhadzadeh@stonybrook.edu (A. Farhadzadeh)

Characterizing incipient motion of low fines content soils with varying compositions, water contents, and relative densities

Abstract

Laboratory flume experiments were conducted to quantify the effects of the soil characteristics on the critical shear stress of low fines content soil samples collected from the Montauk shores in New York. The collected soils were reconstituted at five different fines contents, ranging between 0 and 20%. These soil mixtures were composed of two initial water contents, dry of optimum and optimum moistures, and two relative densities, one moderate dense and the other dense. The strength indices of the soils, including the effective cohesion and effective angle of internal friction, were measured using the consolidated undrained (CU) triaxial test. The initiation of erosion tests was conducted on the soil mixtures under a unidirectional steady current condition. The near-bed flow velocity, at the onset of erosion, was used to determine the critical velocity and shear stress for each soil sample. The results indicate that the critical shear stress increases with the fines content and effective cohesion. The soils with the optimum initial water contents demonstrate a higher erosion resistance than those with the initial water contents dry of optimum. The higher relative density appears to overshadow the effects of the fines content such that the critical shear stress of the denser soils remains relatively insensitive to the soil composition. The denser soils compacted at the optimum initial water content show the highest resistance against erosion. The critical Shields parameter is modified to include the fines content, relative density, and initial water content.

Keywords: Soil erodibility, Sediment transport, Critical shear stress, Initiation of motion

1. Introduction

Seashores and river bottoms are constantly eroded by the flow processes. Grains of various types, including gravel, sand, silt, and clay, mixed at different ratios and demonstrating varying geomechanical characteristics, are the constituent materials of these eroding land features. Ghazian Arabi et al. (2020a, 2020b) showed that the failure and recession of coastal bluffs composed of low fines content materials are triggered by the downcutting and toe erosion in the swash zone, due to the intermittent wave runup and rundown process which imposes a strong shear stress on the beach and bluff materials. The authors further showed that the rate of erosion and recession of beaches and bluffs is directly related to the fines content and the relative density of their constituent materials. Fine (silt and clay) and coarse (sand and gravel) materials exhibit dramatically different erodibilities (Jacobs et al., 2011; Mitchener & Torfs, 1996) as the erosion is an inherently complex process that involves both mechanical and physico-chemical properties of the soil (Yao et al., 2018). In cohesionless sediments, a balance among the gravity, buoyancy, drag, lift, and intergranular forces acting on the particles, controls the incipient motion. These forces are related to the size, density, shape, and gradation of the particles, as well as the flow condition. For cohesive sediments, on the other hand, the initiation of erosion is primarily controlled by the electrochemical forces among the fine particles (Chen et al., 2018; Ye et al., 2011).

The majority of previous studies were focused primarily on the erosion of either cohesionless or cohesive sediments. Those works resulted in several explanations for the erosion of such soils (e.g., Beheshti & Ataie-Ashtiani, 2008; Briaud et al. 1999; Chien & Wan, 1999; Hanson, 1990; Kamphuis & Hall, 1983; Molinas & Hosni, 1999; Zhu et al., 2008). In reality, however, sediments are a combination of cohesionless and cohesive materials, found, for example, in forms of sand–mud mixtures in mudflats and riverbeds.

Several experimental studies were conducted on the erosion of mud–sand mixtures (Jacobs et al., 2011; Mitchener & Torfs, 1996; van Ledden et al., 2004). Some researchers tried, for example, to modify the Shields diagram for sand–mud mixtures (Soulsby & Whitehouse, 1997; Ye et al., 2011). Parameters considered in most of those studies were limited to the mud content and packing, as they were identified to play a critical role in the erodibility of sand–mud mixtures. Mitchener and Torfs (1996) observed that the erosion resistance of sand–mud mixtures is higher than the erosion resistance of each of these materials, separately. They concluded that the mud content ranging between 3% and 15% alters the soil erosion behavior from cohesionless to cohesive. This conclusion was supported by the findings of van Ledden et al. (2004) and Jacobs et al. (2011). Dong (2007) proposed a two-fraction formula for the critical shear stress of cohesionless sand and silt mixtures. Van Rijn (1993) and Whitehouse et al. (2000) developed relationships between the mud content of soils containing less than 20% mud and their critical shear stresses. Van Ledden et al. (2004) and Ahmad et al. (2011) developed two sets of formulae for the erosion of sand–mud mixtures. Van Ledden et al. (2004) introduced a critical mud content based on which the soil behavior can be separated into cohesive and cohesionless. They stated that a mud fraction greater than the critical mud content, transitions the soil behavior to cohesive. Ahmad et al. (2011) proposed a simpler formula for the erosion of sand–mud mixtures, excluding the critical mud content concept. Gao et al. (2021) argued that the critical shear stress of the soil mixtures is related to the mud content, median diameter of the cohesionless soil, and void ratio of the mixture, among others. They proposed an empirical formula for the critical shear stress of the soil mixtures, as a function of the critical shear stress of pure mud, critical shear stress of cohesionless material, and mud content.

The shear strength of soils composed of sand and fine-grained materials varies, among other factors, with the water content which significantly influences the electrochemical forces among the fine particles (Davidson et al., 1962; Loto & Adebayo, 1990). Further, the water content can induce matric suction and apparent cohesion in unsaturated soils (Fredlund et al., 1996). Ye et al. (2011) concluded that the packing condition of artificially generated soil mixtures and the consolidation history of naturally deposited sediments influence their erosion resistance and that a soil with a higher bulk density demonstrates a greater critical shear stress (Ye, 2012). Mohr et al. (2018) established a correlation between the permeability and erosion rate of marine sediments.

Compaction density and water content was found to influence the progression of erosion due to piping and internal erosion of embankments (Fell et al., 2003). Hanson and Hunt (2007) performed jet erosion tests on soil samples of different textures compacted at various water contents and efforts. They concluded that soils' texture and plasticity can influence their erosion resistance no less than the compaction factors. Headcut migration rates following overtopping were increased significantly for soils of different materials and water contents compacted at an equivalent effort (Hahn et al., 2000). It was shown that the soil compaction can significantly affect the rate of erosion and breach of an embankment induced by overflow and overtopping (Fell et al., 2003; Hassan et al., 2004). Wilson et al. (2020) studied the effects of soil consolidation by wetting and drying cycles, on the erosion of predominantly fine-grained soils collected from three sites in Mississippi and one site in Kansas both in the USA. They concluded that the wetting and drying changed the soil physical properties including its consolidation degree. However, the authors were unable to find consistency in changes in the erodibility and critical shear stress among the soil series.

Despite numerous efforts, the state of knowledge on the influence of the geomechanical characteristics (e.g., water content, shear strength, consistency limit, density index) of sediments on their erodibility, is still in its infancy. The lack of a comprehensive knowledge is due to the complex and varying behaviors of soils, especially in the presence of a water flow.

In the present study, the effects of fines content, initial water content, and relative density on the erosion characteristics of low fines content soils are studied. The strength indices of the soil, including the effective cohesion and effective angle of internal friction, were determined using the consolidated undrained (CU) triaxial test. The tests were carried out on the soil samples collected from the Montauk shores on Long Island, New York. The initiation of erosion of the soil mixtures of different characteristics was quantified using a set of flume tests under steady uniform flow. Moreover, correlations between the soil's critical shear stress and shear strength—reflected in its effective cohesion—is investigated.

2. Materials and methods

The laboratory works included two components: (1) the soil mechanics tests, and (2) the steady flow flume tests, both of which were carried out at Stony Brook University. The experimental procedures are described below in further detail.

2.1. Preparation and specifications of soil mixtures

A large amount of soil was collected from Montauk (latitude: 41.065, longitude: −71.861) on Long Island, New York, where the steep shores are composed of granular material of low fines content. The site was selected because it includes steep shores and bluffs that are suffering from constant erosion and recession (Fig. 1). The soil was air dried in the laboratory and then sieved to remove gravels and larger aggregates. Subsequently, the soil index properties and strength were determined as elaborated in Ghazian Arabi et al. (2018, 2020b).

Fig. 1. A view of Montauk site where soil samples were collected.

For the initiation of erosion tests for a total of 20 mixtures, consisting of five different ratios of the fine materials to the total weight of the soil sample, ξ_f = 0, 5%, 10%, 15%, and 20%—alternatively represented as the percentage of sand weight to the total weight of the soil sample, ξ_{sa} = 100%, 95%, 90%, 85%, and 80%, were prepared. Fig. 2 shows the grain size distributions (GSD) of the soil mixtures. The plasticity index (PI) of the fine-grained materials ranged between 14.6 and 18.5. The range of the plasticity limit (PL) was between 18.2% and 21.1%, and the liquid limit (LL) varied between 35.7% and 36.7%. The soil mixtures were prepared at two relative densities, D_r = 39% and 68%, and two initial water contents, ω = 7% and the optimum water content (ω_{opt})—the latter varied for the different soil mixtures. The relative densities, D_r = 39% and 68%, are selected to highlight differences in the erosion behaviors of the medium dense and dense soils, respectively (Holtz et al., 2003). The optimum water content of each soil mixture was determined using the standard Proctor test (D698-12e2, 2012). The target characteristics of the soil mixtures were selected to be within the range of the soil properties at the Montauk shores.

Fig. 2. Grain size distributions (GSD) of soil mixtures prepared for initiation of erosion test.

Table 1 summarizes the soil mixtures' compositions, water contents, relative densities, bulk densities (ρ_{b}), effective cohesions (C'), effective angles of internal friction (ϕ'), and their classifications, according to Unified Soil Classification System (USCS). The soils were categorized as either SC (clayey sand) or SP (poorly graded sand). As noted earlier, the shear strength parameters, C' and ϕ', were determined using the CU triaxial test. The soil mixtures with the relative density, $D_{\mathrm{r}} = 39\%$ (Nos. 1–5 and 11–15) and those with $D_{\mathrm{r}} = 68\%$ (Nos. 6–10 and 16–20) are referred hereafter as the looser and the denser soil mixtures, respectively. The soils with the water content, ω = 7%, were compacted at dry of optimum. The lower half of Table 1, corresponding to the samples Nos. 11–20, are associated with the soils compacted at their optimum water contents.

Table 1 shows that the increase of the fines content from 0 to 20% results in the increase of the effective cohesion and decrease of the effective angle of internal friction. The increase of the effective cohesion is more pronounced for the denser soils, prepared at the optimum water contents. On the other hand, the reduction of the effective angle of internal friction is greater for the looser soils with the initial water content dry of optimum.

2.2. Experimental setup and procedure

The initiation of erosion test was conducted on the 20 soil mixtures in a recirculating flume. The open top, glass sidewall Armfield flume was 500 cm long, 7.6 cm wide, and 25 cm deep. Fig. 3 shows the schematic of the flume and experimental setup. A perforated plate was placed at the entrance of the channel to ensure the establishment of a uniform flow in the channel. While the pump could generate a maximum flow velocity of 120 cm/s in the channel, the mean flow velocity during the tests ranged between 16.7 and 76.7 cm/s. The mean flow velocity was controlled by adjusting the flow depth, for a given flow rate, using a weir at the downstream end of the channel. A fake bottom was created using polyethylene panels of 2 cm in thickness, extending over the entire length of the flume except for a 15 cm long section in the middle. This cavity was used as an in-situ mold of 7.6 cm × 2 cm × 15 cm for the test specimens. The thickness of the soil sample was selected, following Ladd (1978), to ensure a consistent and uniform compaction throughout the soil layer.

Fig. 3. Schematic of experimental setup including flume, in-situ mold for soil sample, and measuring instruments (not to scale).

Each soil mixture was oven dried and mixed with a proportional amount of water to the target water content. Then, the soil was poured into the mold—the cavity created in the fake bottom—and compacted to the target density. The surface of the soil was flush with the fake bottom before flow was established in the flume. The flow velocity was gradually adjusted to a steady state condition while the surface of the soil was continuously monitored. The flow rate was increased incrementally to establish a higher steady state velocity if the soil particles remained immobile. This process was continued until the soil particles started to move. The movement of the soil particles was monitored both visually and using a Nortek Vectrino Profiler. The Vectrino profiler, which was mounted above the soil surface, recorded the instantaneous soil surface elevation as well as the near bottom velocity profile. The Signal-to-Noise Ratio (SNR) and Correlation values were checked to ensure that the measurements were reliable. The sampling rates for the bottom elevation and velocity measurements were 10 Hz and 100 Hz, respectively. The velocity profile was measured over a 1.4 cm height, at a resolution of 1 mm, between 4.0 and 5.4 cm below the probe. The distance between the initial bottom elevation and the profiler's probe helped reduce the likely effects of secondary turbulences that might have been induced due to the interactions between the probe and the flow, on the near-bed velocity (Nikora et al., 1998). Thus, the measurement technique could be considered relatively non-intrusive (Gratiot et al., 2000). A GoPro Hero5 Black camera installed on the side of the flume recorded the video of the initiation of erosion as an additional check. To ensure the repeatability of the tests, each test was conducted three times. As an example, Fig. 4 shows the typical measured temporal variations of the bottom elevation, $\Delta y_{\mathrm{b}}(t) = y_{\mathrm{b}}(t) - y_{\mathrm{b0}}$, and near-bed velocity (U) which together were used to detect the initiation of erosion and calculate the critical shear stress. In Fig. 4, the sudden drop of the bottom elevation, following the second rise of the flow velocity, marks the initiation of erosion.

Fig. 4. Typical timeseries for near-bed velocity (U) and bottom elevation change.

3. Results and discussions

The shear stress imposed by the unidirectional steady current on the surface of the sediment layer is the primary cause of the erosion in this experimental study. Estimating the critical shear stress requires measuring the flow velocity in the vicinity of the bottom. For each soil mixture, the near-bed velocity profile was continuously measured during the test using the

Vectrino profiler. The velocity profile corresponding to the onset of erosion was identified in the recorded velocity data for the analysis.

3.1. Velocity profile at onset of erosion and critical shear stress

The velocity profile in a turbulent boundary layer is well-established. The velocity in the viscous sublayer where the viscosity dominates the vertical transport of momentum, has a specific characteristic. In this region ($0 \leq y \leq \delta_s$, δ_s being the thickness of viscous sublayer), the turbulence intensity fades away to zero at the bed level ($y = 0$). Above the viscous sublayer, however, the turbulence becomes the dominant mechanism controlling the vertical transport of momentum. There, the shape of the velocity profile is different from that of the viscous sublayer. The turbulent boundary layer and near-bed velocity profile are influenced by the bed roughness. Above the viscus sublayer ($y > \delta_s$), the velocity profile follows a logarithmic shape which is a function of the friction velocity, u_*, and the bottom roughness.

$$\frac{U}{u_*} = \frac{1}{\kappa} \ln\left(\frac{y}{y_0}\right) \qquad (1)$$

where U is the velocity at an elevation y above the bed, and $\kappa = 0.4$ is the von Kármán's constant.

Christoffersen and Jonsson (1985) developed an expression for y_0 which is consistent with the experimental results by Nikuradse (1933) who showed that when the surface roughness is smaller than the thickness of the viscus sublayer, the flow above the viscus sublayer is not affected by the surface roughness.

$$y_0 = \frac{k_s}{30}\left(1 - \exp\left(\frac{-u_* k_s}{27\nu}\right)\right) + \frac{\nu}{9u_*} \qquad (2)$$

where k_s is the Nikuradse roughness height, and ν is the kinematic viscosity of water.

Eq. (2) is valid for all flow regimes—those are hydrodynamically smooth, transitional, and rough flows. The hydrodynamically rough turbulent flow is defined as

$$Re_* = \frac{u_* k_s}{\nu} > 70 \tag{3}$$

The transitional turbulent flow is expressed as

$$5 < Re_* < 70 \tag{4}$$

The smooth turbulent flow is stated as

$$Re_* < 5 \tag{5}$$

where Re_* is the roughness Reynolds number.

There are different approaches to estimate the shear velocity and shear stress. For example, Bergeron and Abrahams (1992) recommend intercepting the logarithmic velocity profile with the y axis to determine the roughness length, y_0, while other researchers such as Wilcock (1996) proposed alternative approaches such as using a near-bed velocity and calculating for u_* and y_0 by iterating Eqs. (1) and (2). Here, in order to compare the present results with similar works focusing on mixed sandy and cohesive soils, the latter approach used by the respective researchers (Christoffersen & Jonsson, 1985; Kamphuis & Hall, 1983; Soulsby & Whitehouse, 1997; Ye et al., 2011) is adopted, for consistency. Hence, flow velocity at 4 mm above the bed surface, from the fitted logarithmic profile, was used as the reference near-bed velocity. The Nikuradse roughness $k_s = 2.5D_{50}$ was adopted (Nairn, 1998; Soulsby, 1997; van Rijn, 1984). Since D_{50}, the median grain size, decreases with the increase of the fine-grained material in the soil mixture—also reflected in Table 2—the adopted effective roughness is subsequently reduced. This is consistent with the observations by Das et al. (2019) who studied the surface roughness of sand-clay bottoms using scanning electron microscope (SEM) and 3D profilometer. Das et al. (2019) showed that the surface roughness reduces with the amount of clay material which, in turn, diminishes the turbulent velocity oscillations.

The turbulent flow is identified as transitional for all cases, except for Case C0L, which is smooth. Fig. 5 shows the fitted logarithmic velocity profile and the measured velocity data at the onset of erosion for each soil mixture. The measured velocity data shown in this figure correspond to the three trials. The normalized standard deviation—the coefficient of variation ($\mathrm{CV_U}$) of the near-bed velocity data for the three repetitions is less than 3% for all test cases which indicates the repeatability of the tests. The velocity is normalized by the mean (bulk) flow velocity, $\overline{U}$, and the vertical coordinate, y, is normalized by the steady state flow depth, d.

The critical shear stress, τ_{cr} , is expressed as

$$\tau_{\mathrm{cr}} = \rho u_*^2 \qquad (6)$$

where ρ is the density of water. The calculated critical shear stresses are listed in Table 2.

Fig. 5. Normalized measured velocity and fitted logarithmic velocity profile at onset of erosion for 20 soil mixtures. Panels (a)–(t) correspond to soil samples 1–20 in Table 2, respectively. Measured velocity includes three trials.

3.2. Critical shear stress

The dimensionless critical shear stress of the soil mixture—the critical Shields parameter—θ_{cr} which is a function of the dimensionless grain diameter, D_* (van Rijn, 1984) is presented as

$$\theta_{\mathrm{cr}} = \frac{\tau_{\mathrm{cr}}}{(\rho_{\mathrm{s}} - \rho) g D_{50}} \tag{7}$$

$$D_* = \left[\frac{g(s-1)}{\nu^2}\right]^{\frac{1}{3}} D_{50} \tag{8}$$

where ρ_{s} is the density of the sediment, g is the gravitational acceleration, and $s = \rho_{\mathrm{s}}/\rho$ is the specific gravity of the sediment.

Table 2 summarizes the critical Shields parameters and the dimensionless grain diameters, along with the turbulent flow characteristics for the 20 soil mixtures. Fig. 6 visualizes the present data, together with the data from other researchers, in the Shields diagram modified by Ye (2012). Overall, the critical Shields parameters for the present data appear to agree with the Shields diagram presented by Ye (2012), except for Case C0L. The slight deviation of the present data from the Shields diagram can be due to various factors including the degree of consolidation and interparticle forces in the soil as noted by Panagiotopoulos et al. (1997). The critical Shields parameters for Cases C0L, C5L, C10L, C15L, and C20L, with the lower relative density and the initial water content dry of optimum, fall mainly around the lower band of the Shields diagram. On the other hand, the Shields parameters of Cases WC0D, WC5D, WC10D, WC15D, and WC20D which have the higher density and prepared at the optimum water contents, are within the upper band. The results demonstrate that the soil mixtures prepared at the optimum water contents exhibit a higher erosion resistance compared to those prepared at the 7%

water content, dry of optimum. Fig. 6 shows that the soils of a smaller dimensionless grain size (D_*) exhibit a higher value of the Shields parameter. As reflected in Table 2, the smaller grain size is associated with a larger fines content. Thus, the increase of fines content in the soil mixture leads to a higher Shields parameter.

Fig. 6. (a) Shields diagram updated with present data (filled triangles in black square box), (b) magnified visualization of Shields diagram from present study. Red triangles correspond to Case C0L, C5L, C10L, C15L, and C20L; blue triangles are associated with Cases C0D, C5D, C10D, C15D, and C20D; green triangles represent Cases WC0L, WC5L, WC10L, WC15L, and WC20L; and, purple triangles are related to Cases WC0D, WC5D, WC10D, WC15D, and WC20D.

3.3. Correlations between critical shear stress and soil properties

Fig. 7 shows the critical shear stress as a function of the soil's fines content—the soil composition indicator—and the effective cohesion, which is a strength index. The correlation between the effective cohesion and critical shear stress is similar to that of the fines content and critical shear stress. From Table 2, it becomes clear that the effective cohesion increases with the fines content, relative density, and increase of the water content to the optimum value. Thus, in the following, the critical shear stresses of the soils are discussed with respect to these important soil characteristics—which are interrelated.

The critical shear stress increases with fines content. This is more pronounced in the looser soils (i.e., Cases C0L, C5L, C10L, C15L, and C20L, and Cases WC0L, WC5L, WC10L, WC15L, and WC20L). A higher critical shear stress can be observed for the soils compacted at the optimum water contents (i.e., Cases WC0L, WC5L, WC10L, WC15L, WC20L, and Cases WC0D, WC5D, WC10D, WC15D, and WC20D) compared to those with the water content, dry of optimum (i.e., Cases C0L, C5L, C10L, C15L, and C20L, and Cases C0D, C5D, C10D, C15D, and C20D). This elevated erosion resistance can be attributed to the electrochemical bond among the fine particles and water molecules which leads to the formation of electrical double layers (EDL) around the clay particles (Chen et al., 1994; Mehta & McAnally, 2008). The bond is created through a water membrane forming among the fine particles and, as a result, the strength of the membrane is tied to the water content. As a result, a higher shear stress is required for detaching and dislodging the particles from their positions in the soil fabric, resulting in a higher critical shear stress.

Fig. 7. Critical shear stress vs. fines content and effective cohesion for different soil mixtures. Black markers and lines represent data, and fitted curve corresponding to critical shear stress (vertical axis) vs. fines content (lower horizontal axis), and gray markers and lines represent data and fitted lines for critical shear stress vs. effective cohesion (upper horizontal axis). Triangles represent Cases C0L, C5L, C10L, C15L, and C20L, diamonds indicate Cases C0D, C5D, C10D, C15D, and C20D, circles are associated with Cases WC0L, WC5L, WC10L, WC15L, and WC20L, and squares correspond to Cases WC0D, WC5D, WC10D, WC15D, and WC20D.

For the soil samples that are dry of optimum (ω = 7%), both bulk density and relative density are constant for the soils of varying fines content—this is reflected in Table 1 where the bulk densities for D_r= 39% and 68% are ρ_b = 1,776 and 1,927 g/cm^3, respectively. Therefore, the soil erosion resistance seems to vary consistently with the increase of both the relative density and bulk density. Such a conclusion, however, cannot be made for the soils compacted at their optimum moistures. While for Cases WC0L (No.11) through WC20D (No. 20), the bulk density continuously increases with the increase of the fines content, the erosion resistance of the denser soils (i.e., WC0D–WC20D) remains relatively constant. One the other hand, the erosion resistance of Cases WC0L–WC20L show an increasing trend with the bulk density. As a result, although, the bulk density is an important soil characteristic, its effect on the critical shear stress of the soils of various fines content and initial water content seems inconsistent. Overall, the erosion resistance of the denser soils is not as significantly influenced by the amount of the fine-grained material in the sample as that in the looser soils.

The denser soils exhibit a greater erosion resistance because the incipient motion of the particles, in a molded soil mixture, depends greatly on the particles packing. On other hand, the critical shear stress decreases with the reduction of the relative density, leading to a lower resistance against the erosion because of the lower particle packing. While increasing the fines content from 0 to 20%, in the looser soil with the water content dry of optimum, leads to 1,200% increase in the critical shear stress, the denser soils demonstrate approximately a 20% increase. However, the effects of the fines content on the soils prepared at the optimum water content are quite different. The critical shear stress of the looser soils increases more than 640% when the fines content increases from 0 to 20%. The denser soil, on the other hand, is almost insensitive to the material composition. Such changes of behavior can impact the performance of, for example, earthen dam and levees during an overflow event as reported by Hassan et al. (2004). In fact, the water content together with compaction effort were proved to drastically influence the incipient motion of predominantly sandy soils. A similar conclusion was made based on the results of jet erosion tests on soil samples of different textures compacted at different water contents and efforts reported by Hanson and Hunt (2007). They further concluded that compacting the soil near the optimum water content creates the most erosion-resistant structure.

As discussed, the data presented in Fig. 7 show varying trends for the critical shear stress of the soil mixtures, depending on their compositions and strength indices. To integrate all these parameters into the critical shear stress, both linear and nonlinear regression analyses were performed using Matlab2018a®, by considering different terms comprising the fines content, relative density, and initial water content. The coefficient of determination, R^2, and Nash–Sutcliffe (Nash & Sutcliffe, 1970) model efficiency coefficient (NSE) were used as the metrics for the goodness of the fit. It was concluded that the regression including linear variables could not lead to an accurate representation of the critical Shields parameter, in terms of the soil properties—perhaps due to the inherently interrelatedness of the soil composition, water content, and relative density. Thus, the nonlinear multiple regression method is used. The sensitivity of the resulting θ_{cr} to the various combinations of fines content, water content, relative density, and their pairwise multiplication were analyzed. Table 3 lists R^2 for all combinations considered. The table shows that Combination No. 6 yielded the highest R^2. The result is a predictive relationship (Eq. (9)) for the dimensionless critical shear stress (i.e., the Shields parameter) that exhibits the strongest correlation with the measured data ($R^2 = 0.93$ and NSE = 0.92).

$$\theta_{\mathrm{cr}} = 0.05 + 0.006\xi_{\mathrm{f}}(1 - 0.019D_{\mathrm{r}} + 0.043\omega) - 0.002D_{\mathrm{r}}(1 - 0.231\omega) - 0.012\omega \quad (9)$$

The variables in Eq. (9) are in percentage. The intercept (i.e., 0.05) satisfies the critical shear stress of the loose dry sand with a median diameter, $D_{50} = 0.35$ mm (alternatively, $D_* = 8.3$), based on (Shields, 1936). Eq. (9) is valid for $\omega \leq \omega_{\mathrm{opt}}$. Fig. 8 depicts the comparison of the measured and predicted θ_{cr} using Eq. (9).

Fig. 8. Comparison of measured and predicted dimensionless critical shear stress (i.e., Shields parameter).

4. Conclusions

In this study, twenty mixtures of sand and fine-grained material, with five fines contents (ξ_f = 0, 5%, 10%, 15%, and 20%), two relative densities ($D_r =$ 39% and 68%), and two water contents ($\omega = 7\%$ and the optimum water content of each soil mixture), were prepared and their shear strength parameters were determined using the Consolidated Undrained (CU) triaxial tests.

The critical shear stress of the sediment mixtures was determined under steady state currents in a recirculating flume. This was done by measuring the near-bed current velocity, adopting the logarithmic velocity profile, and calculating the friction velocity at the onset of particle movement. The critical shear stress was found to range between 0.02 and 0.7 Pa. The lowest and highest critical shear stresses corresponded to the soil mixture with $D_r =$ 39%, $\xi_f = 0$ and $\omega = 7\%$, and the soil of $D_r =$ 68%, $\xi_f =$ 20% $\omega = \omega_{opt}$, respectively. The critical shear stress is found to linearly increase with the fines content for the soils of a given water content and relative density. Furthermore, the soils compacted at their optimum initial water content, in general, demonstrate a higher resistance against erosion compared to those with the initial water content dry of optimum. The higher relative density appears to overshadow the effects of the fines content such that the critical shear stresses of the denser soils remain relatively insensitive to the soil composition. The denser soils with the optimum initial water contents show the highest resistance against erosion. Further, the trends of the variation of the critical shear stress with the fines content and the effective cohesion are alike—the critical shear stress increases with the fines content and effective cohesion. Finally, an empirical relationship has been developed by modifying the critical Shields parameter to include the fines content, relative density, and initial water content of the soil.

This work, which is among the very few studies on the effects of the geomechanics on the erosion behavior of sediment mixtures, provides a quantitative analysis describing the significance of the composition and strength indices for the initiation of erosion of predominantly sandy soils. The presented findings can lead to a better understanding of the erosion of riverbeds and banks, as well as beaches and soft bluffs with constituent materials that are mixtures of sand and fine-grain materials. The failure of coastal bluffs, for example, is initiated by foreshore downcutting and erosion of the bluff toe by swash flow and wave runup actions. An accurate estimation of the rate of recession, critical for coastal planning and development, cannot be done without a quantitative assessment of the erosion processes.

The prediction of the soil erodibility and erosion rate requires more comprehensive research, encompassing a broader range of soil characteristics, beyond those investigated in the present work, as soils behavior may drastically vary due to the heterogeneity in the properties, arising from the soil's origin and history. In addition, the scale effect including the effect of soil disturbance on the erosion of the soils of different compositions and mechanical strengths need to be considered in future studies.

Data availability statement

Some or all data, models, or code that support the findings of this study are available from the corresponding author upon reasonable request. The velocity data and soil characteristics are available at: Farhadzadeh and Ghazian Arabi (2020), "Soil erodibility data", Mendeley Data, V2, DOI: 10.17632/n6zwshnfhg.2.

Acknowledgement

This study was funded by National Oceanic and Atmospheric Administration, New York Sea Grant, Award No. 80794.

References

Ahmad, M., Dong, P., Mamat, M., Nik, W., & Mohd, M. (2011). The critical shear stresses for sand and mud mixture. *Applied Mathematical Sciences*, 53–71.

Beheshti, A., & Ataie-Ashtiani, B. (2008). Analysis of threshold and incipient conditions for sediment movement. *Coastal Engineering*, 423–430.

Bergeron, N., & Abrahams, A. (1992). Estimating shear velocity and roughness from velocity profiles. *Water Resources Research*, 2155–2158.

Briaud, J.-L., Ting, F. C., Chen, H. C., Gudavalli, R., Perugu, S., & Wei, a. G. (1999). SRICOS: Prediction of scour rate in cohesive soils at Bridge Piers. *Journal of Geotechnical and Geoenvironmental Engineering, 125*(4).

Chaudhuri, S., & Debnath, K. (2013). Observations on initiation of pier scour and equilibrium scour hole profiles in cohesive sediments. *ISH journal of hydraulic engineering, 19*(1).

Chen, D., Wang, Y., Melville, B., Huang, H., & Zhang, W. (2018). Unified formula for critical shear stress for erosion of sand, mud, and sand-mud mixtures. *Journal of Hydraulic Engineering*, 1–14.

Chen, Z., Zhou, J., & Wang, H. (1994). *Soil mechanics.* Tsinghua University Press.

Chien, N., & Wan, Z. (1999). *Mechanics of sediment transport.* American Society of Civil Engineers.

Christoffersen, J. B., & Jonsson, I. (1985). Bed friction and dissipation in a combined current and wave motion. *Ocean Engineering* , 387–423.

Christoffersen, J. B., & Jonsson, I. G. (1985). Bed friction and dissipation in a combined current and wave motion. *Ocean Engineering*, 387–423.

D698-12e2, A. (2012). *Standard Test Methods for Laboratory Compaction Characteristics of Soil Using Standard Effort.* American Society for Testing and Materials.

Das, V. K., Roy, S., Barman, K., Chaudhuri, S., & Debnath, K. (2019). Study of clay–sand network structures and its effect on river bank erosion: An experimental approach. *Environmental Earth Sciences*, 1–18.

Davidson, D. T., Pitre, G. L., Mateos, M., & George, K. P. (1962). Moisture-density, moisture-strength and compaction characteristics of cement-treated soil mixtures. *41st Annual Meeting of the Highway Research Board.* Washington DC.

Dong, P. (2007). Two-fraction formulation of critical shear stresses for sand and silt mixtures. *Journal of Waterway, Port, Coastal and Ocean Engineering*, 238–241.

Fell, R., Wan, C. F., Cyganiewicz, J., & Foster, M. (2003). Time for development of internal erosion and piping in embankment dams. *Journal of Geotechnical and Geoenvironmental Engineering*, 307–314.

Fredlund, D. G., Xing, A., Fredlund, M. D., & Barbour, S. L. (1996). The relationship of the unsaturated soil shear strength to the soil-water characteristic curve. *Canadian Geotechnical Journal*, 440–448.

Gao, X., Wang, Q., Xu, C., & Su, R. (2021). Experimental study on critical shear stress of cohesive soils and soil mixtures. *Transactions of the ASABE*, 587–600.

Ghazian Arabi, M., Farhadzadeh, A., & Khosravi, A. (2018). Recession of predominantly sandy bluffs. *36th International Conference on Coastal Engineering (ICCE2018).* Baltimore: ASCE.

Ghazian Arabi, M., Farhadzadeh, A., & Khosravi, M. (2020a). Erosion and recession of beach-bluff system due to wave and surge actions. *Geo-Congress 2020.* Minneapolis: ASCE.

Ghazian Arabi, M., Khosravi, M., & Farhadzadeh, A. (2020b). Effects of fines content and relative density on erosion and recession of predominantly sandy beach-bluff System. *Journal of Waterway, Port, Coastal, and Ocean Engineering*.

Gratiot, N., Mory, M., & Auchère, D. (2000). An acoustic Doppler velocimeter (ADV) for the characterisation of turbulence in concentrated fluid mud. *Continental Shelf Research*, 1551–1567.

Hahn, W., Hanson, G., & Cook, K. (2000). Breach morphology observations of embankment overtopping tests. *Joint Conference on Water Resource Engineering and Water Resources Planning and Management* . Minnesota: ASCE.

Hanson, G. J. (1990). Surface erodibility of earthen channels at high stresses part I - Open channel testing. *Transactions of the ASAE, 33*(1), 127–131.

Hanson, G. J., & Hunt, S. L. (2007). Lessons learned using laboratory JET method to measure soil erodibility of compacted soils. *Applied Engineering in Agriculture*, 305–312.

Hassan, M., Morris, M., Hanson, G., & Lakhal., K. (2004). Breach formation: Laboratory and numerical modeling of breach formation. *Proc. Dam Safety.* Lexington, Ky: Association of State Dam Safety Officials (ASDSO).

Holtz, R., Kovacs, W., & Sheahan, T. (2003). *An introduction to geotechnical engineering.* Upper Saddle River, NJ: Prentice-Hall .

Jacobs, W., Le Hir, P., van Kesteren, W., & Cann, P. (2011). Erosion thresholds of sand-mud mixtures. *Continebntal Shelf research*, S14–S25.

Kamphuis, W. J. (1990). Influence of sand or gravel on the erosion of cohesive sediment. *J Hydr Res, 28*(1), 43–53.

Kamphuis, W., & Hall, K. (1983). Cohesive material erosion by unidirectional current. *J Hydr Eng, 109*(1), 49–61.

Ladd, R. (1978). Preparing test specimens using undercompaction. *Geotechnical Testing Journal* , 16–23.

Lick, W. J. (2004). Initiation of movement of quartz particles. *Journal of Hydraulic Engineering*, 755–761.

Loto, C., & Adebayo, H. (1990). Effects of variation in water contents, clay fraction and sodim carbonate additions on the synthetic moulding properties of Igbokoda clay and silica sand. *Applied Clay Science*, 165–181.

Mehta, A., & McAnally, W. (2008). Fine grained sediment transport. In M. Garcia, *Sedimentation engineering: processes, Measurements, modeling, and practice* (pp. . 253–306). American Society of Civil Engineers.

Mitchener, H., & Torfs, H. (1996). Erosion of mud/sand mixtures. *Coastal Engineering, 29*(96), 1–25.

Mohr, H., Draper, S., White, D., & Cheng, L. (2018). The influence of permeability on the erosion rate of fine-grained marine sediments. *Coastal Engineering*, 124–135.

Molinas, A., & Hosni, M. M. (1999). *Effects of gradation and cohesion on bridge scour: Volume 4: Experimental study of scour around circular piers in cohesive soils.* Turner-Fairbank Highway Research Center ;United States. Federal Highway Administration.

Nairn, B. (1998). *Incipient Transport of Silt-Sized Sediments.* Pasadena, California: W.M. Keck Laboratory of Hydraulics and Water Resources.

Nash, J., & Sutcliffe, J. (1970). River flow forecasting through conceptual models, part I — A discussion of principles. *Journal of Hydrology*, 282–290.

Nielsen, A. W., Sumer, B. M., Ebbe, S. S., & Fredsøe, J. (2012). Experimental Study on the Scour around a Monopile in Breaking Waves. *Journal of Waterway, Port, Coastal, and Ocean Engineering, 138*(6).

Nikora, V. I., Suren, A. M., Brown, S. L., & Biggs, B. J. (1998). The effects of the moss Fissidens rigidulus (Fissidentaceae: Musci) on near-bed flow structure in an experimental cobble bed flume. *Limnology and Oceanography*, 1321–1331.

Nikuradse, J. (1933). *Laws of flow in rough pipes.* VDI Forschungsheft 361. Also NACA TM 1292.

Panagiotopoulos, I., Voulgaris, G., & Collins, M. B. (1997). The influence of clay on the threshold of movement of fine sandy beds. *Coastal Engineering*, 19–43.

Rambabu, M., Rao, S., & Sundar, V. (2003). Current-induced scour around a vertical pile in cohesive soil. *Ocean Eng., 30*(4), 893–920.

Shields, A. (1936). *Application of similarity principles and turbulence research to bed-load movement, (English translation of the original German manuscript).* Pasadena: Hydrodynamics Laboratory. California Institute of Technology.

Soulsby, R. (1997). *Dynamics of marine sands: A manual for practical applications.* Thomas Telford Publishing.

Soulsby, R., & Whitehouse, R. (1997). Threshold of sediment motion in coastal envinroment. *Combined Australasian Coastal Engineering and Port Conferences.* Christchurch: University of Canterbury.

van Ledden, M., Van Kesteren, W. G., & Winterwerp, J. C. (2004). A conceptual framework for the erosion behaviour of sand-mud mixtures. *Continental Shelf Research*, 1–11.

van Rijn, L. (1984). Sediment transport part I: Bed load transport. *Journal of Hydraulic Engineering*, 1431–1456.

van Rijn, L. (1993). *Principles of sediment transport in rivers, estuaries and coastal seas.* Amsterdam: Aqua publications.

Whitehouse, R., Soulsby, R., Roberts, W., & Mitchener, H. (2000). *Dynamics of estuarine muds. In dynamics of estuarine muds.* Delft: Thomas Telford,.

Wilcock, P. (1996). Estimating local bed shear stress from velocity observations. *Water Resources Research*, 3361–3366.

Wilson, G., Zhang, T., Wells, R., & Liu, B. (2020). Consolidation effects on relationships among soil erosion properties and soil physical quality indicators. *Soil and Tillage Research*.

Yao, P., Hu, Z., Su, M., Chen, Y., & Ou, S. (2018). Erosion Behavior of sand-silt mixtures: the role of silt content. *Journal of Coastal Research*, 1171–1175.

Ye, Z. (2012). *Erosion threshold and erosion rate of seabed sediments.* The University of Western Australia.

Ye, Z., Cheng, L., & Zang, Z. (2011). Experimental study of erosion threshold of reconstituted sediments. *Proceedings of the International Conference on Offshore Mechanics and Arctic Engineering*, (pp. 973–983). Rotterdam.

Zhu, Y., Lu, J., Liao, H., Wang, J., Fan, B., & Yao, S. (2008). Research on cohesive sediment erosion by flow: An overview. *Science China Technological Sciences*, 2001–2012.

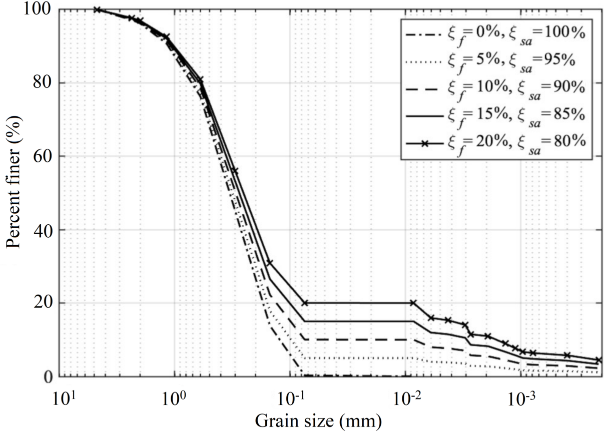
Percent finer (%)
Grain size (mm)
100
80
60
40
20
0
10^1
10^0
10^-1
10^-2
10^-3
ξ_f = 0%, ξ_sa = 100%
ξ_f = 5%, ξ_sa = 95%
ξ_f = 10%, ξ_sa = 90%
ξ_f = 15%, ξ_sa = 85%
ξ_f = 20%, ξ_sa = 80%

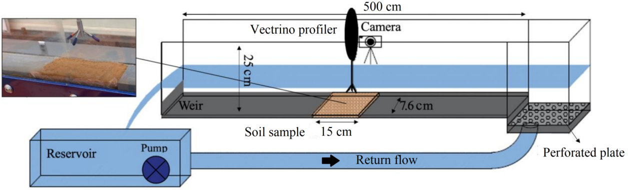

500 cm
Vectrino profiler
Camera
25 cm
Weir
7.6 cm
Soil sample
15 cm
Reservoir
Pump
Return flow
Perforated plate

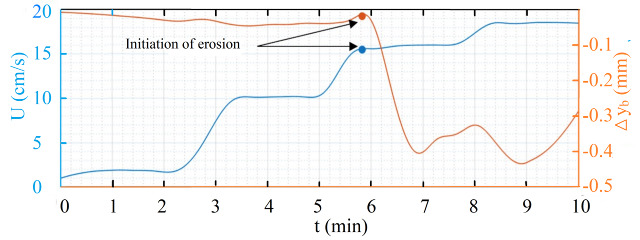

Initiation of erosion
U (cm/s)
0
5
10
15
20
Δy_b (mm)
-0.1
-0.2
-0.3
-0.4
-0.5
0
1
2
3
4
5
6
7
8
9
10
t (min)

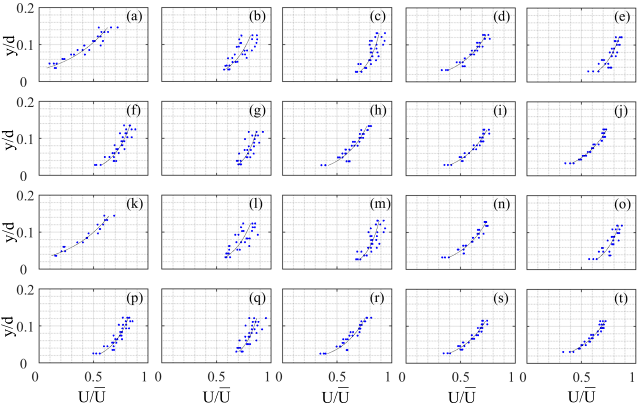

0.2
0.1
0
y/d
(a)
(b)
(c)
(d)
(e)
(f)
(g)
(h)
(i)
(j)
(k)
(l)
(m)
(n)
(o)
(p)
(q)
(r)
(s)
(t)
0
0.5
1
U/$\overline{U}$

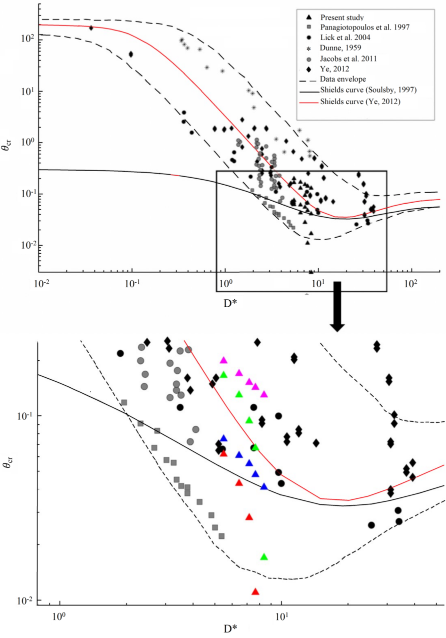
Present study
Panagiotopoulos et al. 1997
Lick et al. 2004
Dunne, 1959
Jacobs et al. 2011
Ye, 2012
Data envelope
Shields curve (Soulsby, 1997)
Shields curve (Ye, 2012)
θ_{cr}
D*
10^{-2}
10^{-1}
10^{0}
10^{1}
10^{2}

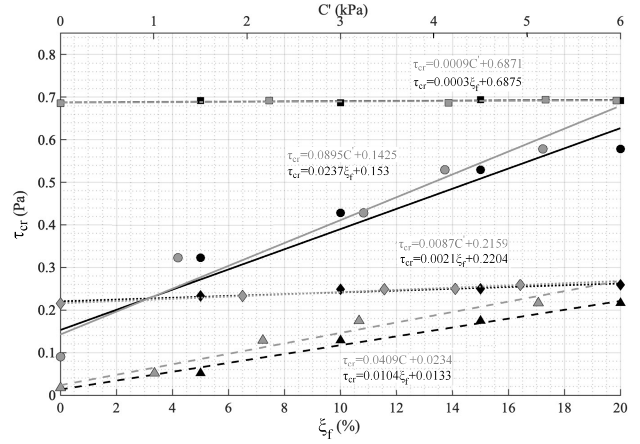

C' (kPa)
0
1
2
3
4
5
6
0.8
0.7
0.6
0.5
0.4
0.3
0.2
0.1
0
τcr (Pa)
τcr=0.0009C'+0.6871
τcr=0.0003ξf+0.6875
τcr=0.0895C'+0.1425
τcr=0.0237ξf+0.153
τcr=0.0087C'+0.2159
τcr=0.0021ξf+0.2204
τcr=0.0409C'+0.0234
τcr=0.0104ξf+0.0133
0
2
4
6
8
10
12
14
16
18
20
ξf (%)

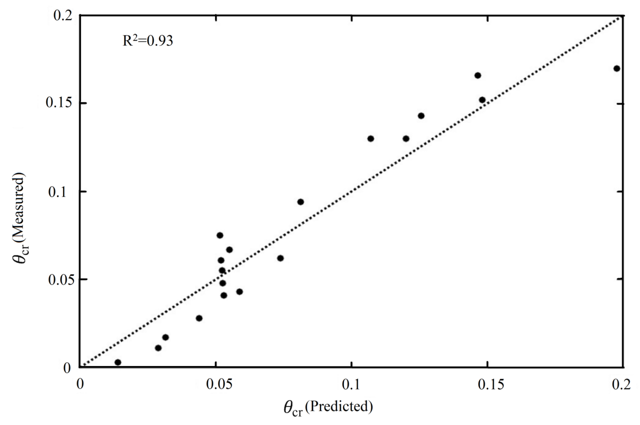
R²=0.93
0.2
0.15
0.1
0.05
0
0
0.05
0.1
0.15
0.2
θ_{cr} (Measured)
θ_{cr} (Predicted)

Table 1. Summary of soil mixtures characteristics for initiation of erosion tests.

No.	Name	ξ_f (%)	ξ_{sa} (%)	ω (%)	D_r (%)	ρ_b (kg/m^3)	C' (kPa)	ϕ'(°)	USCS
1	C0L	0	100	7.0	39	1776	0.00	33.0	SP
2	C5L	5	95	7.0	39	1776	1.01	31.2	SP
3	C10L	10	90	7.0	39	1776	2.17	26.5	SP
4	C15L	15	85	7.0	39	1776	3.20	26.4	SC
5	C20L	20	80	7.0	39	1776	5.12	22.1	SC
6	C0D	0	100	7.0	68	1927	0.00	34.3	SP
7	C5D	5	95	7.0	68	1927	1.95	32.1	SP
8	C10D	10	90	7.0	68	1927	3.47	31.3	SP
9	C15D	15	85	7.0	68	1927	4.23	29.7	SC
10	C20D	20	80	7.0	68	1927	4.93	27.2	SC
11	WC0L	0	100	9.5	39	1817	0.00	33.3	SP
12	WC5L	5	95	10.2	39	1829	1.26	32.8	SP
13	WC10L	10	90	11.0	39	1842	3.25	27.2	SP
14	WC15L	15	85	12.8	39	1872	4.12	26.7	SC
15	WC20L	20	80	13.2	39	1879	5.17	22.4	SC
16	WC0D	0	100	9.5	68	1972	0.00	34.6	SP
17	WC5D	5	95	10.2	68	1985	2.24	32.4	SP
18	WC10D	10	90	11.0	68	1999	4.16	32.3	SP
19	WC15D	15	85	12.8	68	2031	5.20	30.1	SC
20	WC20D	20	80	13.2	68	2039	5.96	27.6	SC

Table 2. Turbulent flow characteristics at onset of erosion and critical Shields parameters for 20 soil samples.

No	Name	D_{50} (mm)	U (cm/s)	CV_U (%)	u_* (cm/s)	Re_*	τ_{cr} (Pa)	D_*	θ_{cr}	d (cm)	$\bar{U}$ (cm/s)
1	C0L	0.35	5.0	2.9	0.4	3.4	0.02	8.3	0.003	8.4	22.2
2	C5L	0.32	9.4	3.2	0.7	5.4	0.05	7.6	0.011	10.0	16.7
3	C10L	0.30	15.5	0.7	1.1	8.1	0.13	7.1	0.028	9.8	20.1
4	C15L	0.27	18.5	2.1	1.3	8.5	0.17	6.4	0.043	9.7	36.6
5	C20L	0.23	21.1	1.9	1.5	8.0	0.22	5.4	0.062	10.0	28.0
6	C0D	0.35	19.7	1.8	1.5	12.2	0.22	8.3	0.041	9.6	29.1
7	C5D	0.32	20.9	2.5	1.5	11.6	0.23	7.6	0.048	10.5	29.7
8	C10D	0.30	21.8	2.5	1.6	11.2	0.25	7.1	0.055	9.7	36.8
9	C15D	0.27	22.2	0.9	1.6	10.1	0.25	6.4	0.061	9.7	431
10	C20D	0.23	23.2	2.1	1.6	8.8	0.26	5.4	0.075	10.0	49.5
11	WC0L	0.35	12.6	9.2	0.9	7.9	0.09	8.3	0.017	8.5	62.2
12	WC5L	0.32	24.5	1.9	1.8	13.7	0.32	7.6	0.067	10.1	41.3
13	WC10L	0.30	28.5	1.7	2.1	14.7	0.43	7.1	0.094	9.8	37.6
14	WC15L	0.27	32.3	0.5	2.3	14.7	0.53	6.4	0.130	9.6	61.4
15	WC20L	0.23	34.8	0.7	2.4	13.1	0.58	5.4	0.166	10.2	46.9
16	WC0D	0.35	34.5	1.2	2.6	21.8	0.69	8.3	0.130	10.6	50.9
17	WC5D	0.32	35.4	1.9	2.6	20.0	0.69	7.6	0.143	10.2	50.8
18	WC10D	0.30	35.8	0.6	2.6	18.7	0.69	7.1	0.152	10.6	61.2
19	WC15D	0.27	36.8	1.7	2.6	16.8	0.69	6.4	0.170	10.5	71.3
20	WC20D	0.23	38.0	1.6	2.6	14.3	0.69	5.4	0.199	11.0	76.7

Table 3. Summary of various combinations and corresponding coefficient of determinations.

No.	ξ_f	D_r	ω	$\xi_f D_r$	$\xi_f \omega$	ωD_r	R^2
1	✓	✓	✓	×	×	×	0.22
2	✓	✓	✓	✓	×	×	0.72
3	✓	✓	✓	✓	✓	×	0.73
4	✓	✓	✓	×	×	✓	0.72
5	✓	✓	✓	×	✓	×	0.47
6	✓	✓	✓	✓	✓	✓	0.93